Analysis and Experiment on Harmonic Current Distortion in Wireless Power Transfer System Using a Diode Rectifier

Katsuhiro Hata, Takehiro Imura, and Yoichi Hori
The University of Tokyo,
5–1–5, Kashiwanoha, Kashiwa, Chiba, 277–8561, Japan
Phone: +81-4-7136-3881, Fax: 81-4-7136-3881
Email: hata@hflab.k.u-tokyo.ac.jp, imura@hori.k.u-toyko.ac.jp, hori@k.u-tokyo.ac.jp

***Abstract*—Wireless power transfer (WPT) via magnetic resonance coupling provides highly efficient mid-range transmission. Its transmitting power can be controlled using a diode rectifier and a DC-DC converter on the secondary side. Previous research replaces the load and the rectifier circuit with an equivalent load resistance or a fundamental harmonic sine wave voltage source to analyze the charging power of WPT. In such a case however, the effect caused by the rectifier circuit becomes unclear because the harmonic components are neglected. As a result, the theoretical charging power and its true value have an error due to the harmonic current distortion. In this paper, a novel WPT circuit model is proposed for the analysis of the harmonic current distortion on the secondary side. The proposed model uses the secondary voltage as the input variable of transfer functions and makes clear the effect caused by the rectifier circuit. Experiments demonstrate that the harmonic current distortion is increased with the increase in the secondary voltage. These results accord with the analysis using the proposed model and verify the effectiveness of the proposed model.**

***Keywords*—Wireless power transfer, Magnetic resonance coupling, Diode rectifier, Harmonic current distortion.**

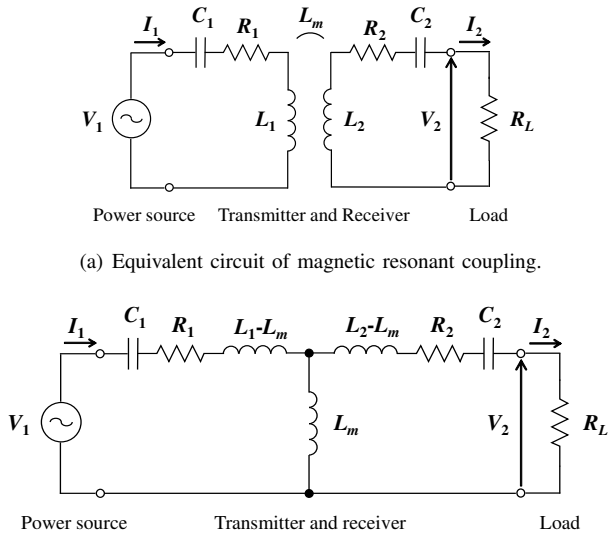

(a) Equivalent circuit of magnetic resonant coupling.

(b) T–type equivalent circuit.

Fig. 1. Equivalent circuit of the wireless power transfer system.

I. Introduction

Electric vehicles (EVs) have environmental advantages and the capacity for advanced motion control due to the fast response time of their electric motors [1]. However, EVs need to be charged frequently due to their limited mileage per charge. Charging operations should be simplified to reduce the burden on the user.

Wireless power transfer (WPT) can mitigate complicated charging operations and apply dynamic charging to EVs in motion [2], [3]. WPT via magnetic resonance coupling provides highly efficient mid-range transmission and it has robustness to misalignment between a transmitter and a receiver [4], [5]. Its transmitting efficiency and its charging power are determined not only by the parameters of the transmitter and the receiver but also by the load [6]. The load condition can be controlled using a diode rectifier and a DC-DC converter on the secondary side [7], [8]. As a result, the transmitting efficiency can be maximized [9], [10] or the charging power can be controlled on the secondary side [11]–[13].

Many papers on the modeling of the WPT circuit use an equivalent load resistance, which includes the load and the rectifier circuit [14]–[16]. A previous study [17] has proposed a fundamental mode equivalent circuit, which replaces the load and the rectifier circuit with a fundamental harmonic sine wave voltage source. Furthermore, the WPT circuit model considering the discontinuous mode of the diode rectifier has been represented [18], [19]. However, the actual load is replaced by an equivalent load resistance or a fundamental harmonic sine wave voltage source. As a result, the effects caused by the diode rectifier cannot be made clear because the harmonic components are neglected. This causes an error in the theoretical charging power of WPT.

This paper proposes a novel WPT circuit model, which is expressed by multi-input, multi-output (MIMO) transfer functions using the secondary voltage as the input variable. The proposed model can analyze the harmonic current distortion caused by the rectifier circuit because the load is not approximated by any elements. Experiments show that the charging power control on the secondary side using the diode rectifier has the potential for causing the harmonic current distortion. This result is analyzed using the proposed model and the effectiveness of the proposed model is verified.

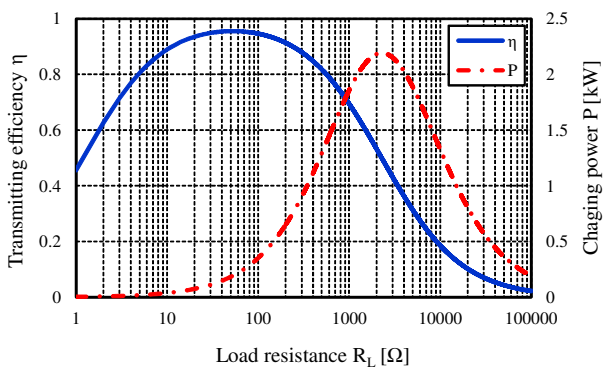

Fig. 2. Load resistance vs. transmitting efficiency and charging power.

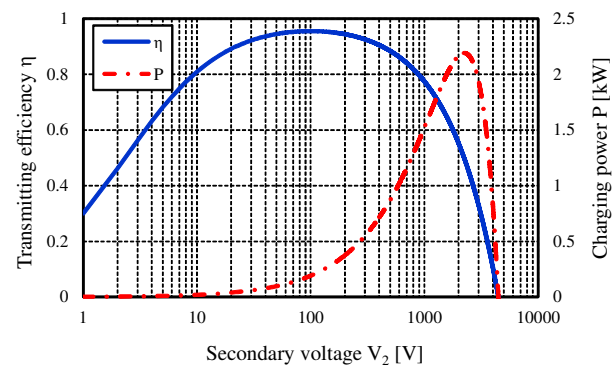

Fig. 3. Secondary voltage vs. transmitting efficiency and charging power.

II. Wireless Power Transfer via Magnetic Resonance Coupling

A. Characteristics at resonance frequency

A series-series circuit topology is used for the wireless power transfer circuit and its equivalent circuit is shown in Fig. 1 [20]. The transmitter and the receiver are characterized by the inductances L_1, L_2, the series-resonance capacitors C_1, C_2, and the internal resistances R_1, R_2, respectively. L_m is the mutual inductance between the transmitter and the receiver. V_1 is the RMS voltage of a power source and its angular frequency is expressed as ω_0. The transmitter and the receiver are designed to satisfy the following equation.

$$\omega_0 = \frac{1}{\sqrt{L_1 C_1}} = \frac{1}{\sqrt{L_2 C_2}} \tag{1}$$

When the load resistance is R_L, the voltage ratio A_V and the current ratio A_I between the secondary-side and the primary-side are expressed as follows:

$$A_V = \frac{V_2}{V_1} = j\frac{\omega_0 L_m R_L}{R_1 R_2 + R_1 R_L + (\omega_0 L_m)^2} \tag{2}$$

$$A_I = \frac{I_2}{I_1} = j\frac{\omega_0 L_m}{R_2 + R_L} \tag{3}$$

where V_2, I_1, and I_2 are the RMS values of the secondary voltage, the primary current, and the secondary current, respectively. Then, the transmitting efficiency η is expressed as follows:

$$\eta = \frac{(\omega_0 L_m)^2 R_L}{(R_2 + R_L)\{R_1 R_2 + R_1 R_L + (\omega_0 L_m)^2\}} \tag{4}$$

and the charging power P is described as follows:

$$P = \frac{(\omega_0 L_m)^2 R_L}{\{R_1 R_2 + R_1 R_L + (\omega_0 L_m)^2\}^2} {V_1}^2. \tag{5}$$

Fig. 2 shows the load resistance R_L versus the transmitting efficiency η and the charging power P. The parameters of the transmitter and the receiver, which are used in this work, are given in TABLE I. The amplitude of V_1 is equal to 100 V. η is maximized if R_L is given as follows:

$$R_{L\eta max} = \sqrt{R_2 \left\{ \frac{(\omega_0 L_m)^2}{R_1} + R_2 \right\}}. \tag{6}$$

TABLE I. Parameters of transmitter and receiver.

	Primary side	Secondary side
Resistance R_1, R_2	1.14 Ω	1.19 Ω
Inductance L_1, L_2	637.9 μH	638.4 μH
Capacitance C_1, C_2	4002 pF	3996 pF
Resonant frequency f_1, f_2	99.6 kHz	99.6 kHz
Mutual inductance L_m	81.5 μH (gap: 200 mm)	
Outer diameter	448 mm	
Number of turns	56 turns	

P is maximized if R_L is expressed as follows:

$$R_{LP\max} = \frac{(\omega_0 L_m)^2}{R_1} + R_2. \tag{7}$$

B. Charging power control on the secondary side

The load resistance R_L is determined by the amplitude of the secondary voltage V_2, which can be controlled by the DC-DC converter on the secondary side. Fig. 3 shows the secondary voltage V_2 versus the transmitting efficiency η and the charging power P. If the maximum efficiency is achieved, V_2 satisfies the following equation [9].

$$V_{2\eta\max} = \sqrt{\frac{R_2}{R_1}} \frac{\omega_0 L_m}{\sqrt{R_1 R_2 + (\omega_0 L_m)^2} + \sqrt{R_1 R_2}} V_1 \tag{8}$$

Charging power control can be achieved by secondary voltage control [12], [13]. However, it is effective only if V_2 is controlled below the maximum secondary voltage $V_{2\max}$, which is expressed as follows:

$$V_{2\max} = \frac{\omega_0 L_m}{R_1} V_1. \tag{9}$$

Then, the equivalent load resistance R_L goes to infinity and the voltage ratio A_V becomes saturated [6]. The maximum power is obtained when V_2 is given as follows:

$$V_{2P\max} = \frac{\omega_0 L_m}{2R_1} V_1 = \frac{V_{2\max}}{2}. \tag{10}$$

For efficient transmission, it is important to define the operating range of V_2 to be below $V_{2P\max}$. As a result, the

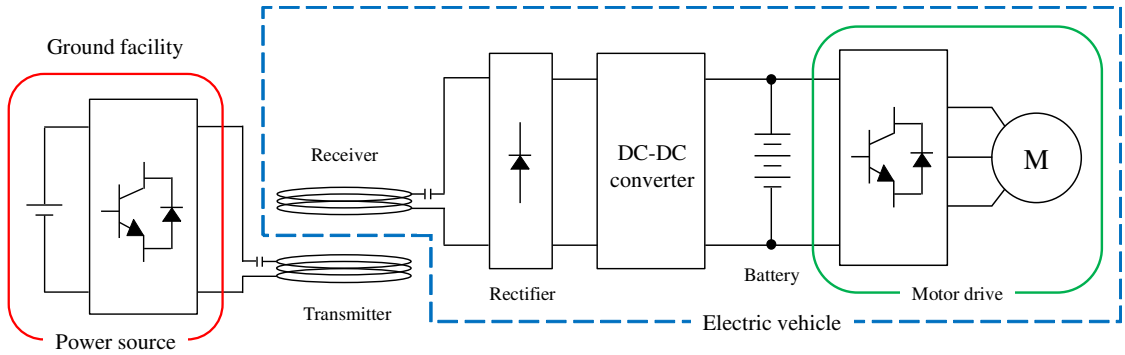

Fig. 4. System configuration of wireless charging for electric vehicle.

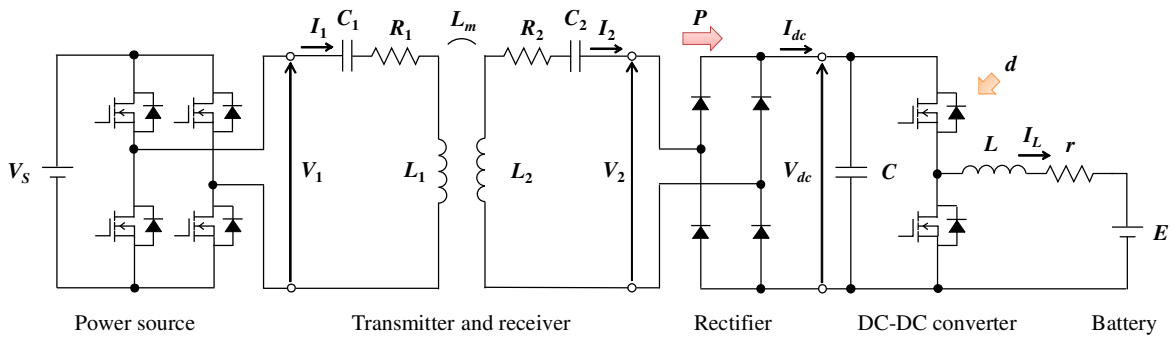

Fig. 5. Circuit diagram of the wireless charging system.

reference voltage ${V_2}^*$, which obtains the desired power P^*, is given as follows [13]:

$$ {V_2}^* = \left(\frac{\omega_0 L_m V_1}{2R_1}\right) - \sqrt{\left(\frac{\omega_0 L_m V_1}{2R_1}\right)^2 - \frac{\{R_1 R_2 + (\omega_0 L_m)^2\}P^*}{R_1}}. \quad (11) $$

C. Effect of the diode rectifier

Fig. 4 shows a system configuration of wireless charging for an EV. Assuming that the voltage control of the DC-DC converter is designed properly, the charging power control can be achieved. The circuit diagram of the wireless charging system is shown in Fig. 5. In this paper, the motor drive system is neglected as this is a fundamental study.

The secondary voltage is generated by the diode rectifier. If the absolute value of the secondary voltage exceeds the amplitude of the DC link voltage V_{dc}, the rectifier is conducted and the absolute value of the secondary voltage becomes the same amplitude as V_{dc}, where the forward voltage of the diode is ignored. Furthermore, if the amplitude of V_{dc} is much lower than the amplitude of $V_{2\max}$, the secondary voltage can be assumed to be a square wave.

On the other hand, in the case where the absolute value of the secondary voltage cannot be larger than the amplitude of V_{dc}, the secondary current cannot flow through the rectifier. Therefore, the secondary current includes the discontinuous state and could not be strictly approximated by the sine wave.

III. Modeling of the Wireless Power Transfer Circuit

A. Conventional model using the equivalent load resistance

Previous research [16] has proposed a transfer function model of the WPT circuit using the equivalent load resistance R_L. Its block diagram is shown in Fig. 6. $Y_{c1}(s)$ and $Y_{c2}(s)$ are transfer functions from the primary voltage $V_1(s)$ to the primary current $I_1(s)$ and the secondary current $I_2(s)$. For the charging power control on the secondary side, this paper focuses on $Y_{c2}(s)$. This is given as follows:

$$ Y_{c2}(s) = \frac{I_2(s)}{V_1(s)} = \frac{b_{c3}s^3}{s^4 + a_{c3}s^3 + a_{c2}s^2 + a_{c1}s + a_{c0}} \quad (12) $$

where each coefficient is defined as follows:

$$ a_{c3} = \frac{R_1 L_2 + (R_2 + R_L)L_1}{L_1 L_2 - {L_m}^2} \quad (13) $$

$$ a_{c2} = \frac{R_1(R_2 + R_L) + (L_1/C_2) + (L_2/C_1)}{L_1 L_2 - {L_m}^2} \quad (14) $$

$$ a_{c1} = \frac{(R_1/C_2) + \{(R_2 + R_L)/C_1\}}{L_1 L_2 - {L_m}^2} \quad (15) $$

$$ a_{c0} = \frac{1}{C_1 C_2 (L_1 L_2 - {L_m}^2)} \quad (16) $$

$$ b_{c3} = \frac{-L_m}{L_1 L_2 - {L_m}^2}. \quad (17) $$

The bode diagram of $Y_{c2}(s)$ is shown in Fig. 7. In this model, it is difficult to analyze the harmonic current distor-

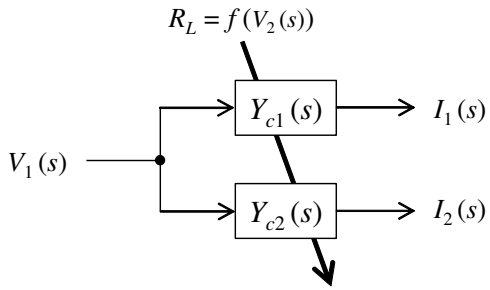

Fig. 6. Block diagram of the conventional model.

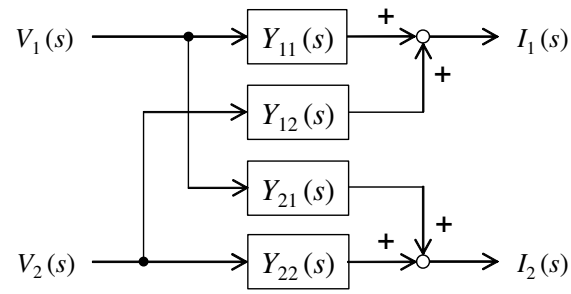

Fig. 8. Block diagram of the proposed model.

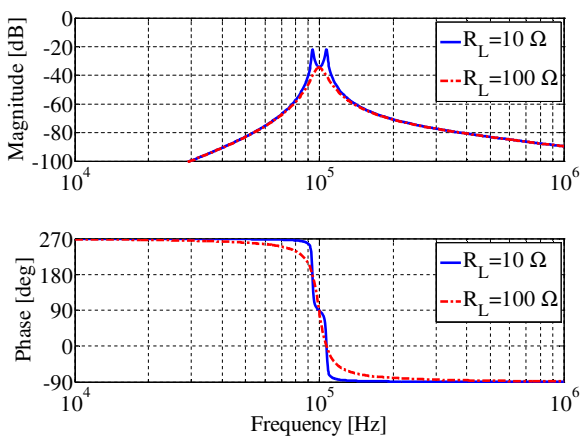

Fig. 7. Bode diagram of the conventional transfer function Y_{c2}.

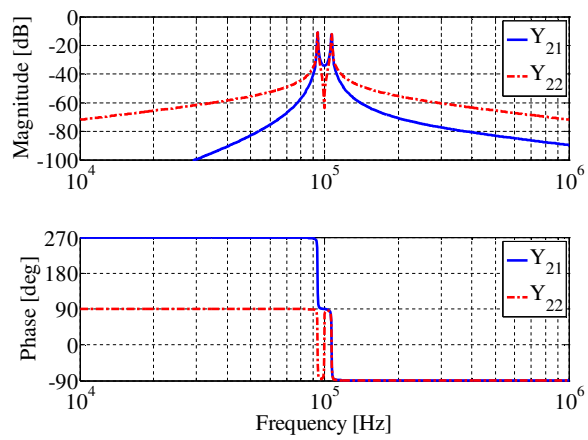

Fig. 9. Bode diagram of the proposed transfer functions Y_{21} and Y_{22}.

tion because the bode diagram is changed by R_L, which is controlled to achieve the desired charging power.

B. Proposed model using the secondary voltage as an input variable

This paper proposes a transfer function model of the WPT circuit using the secondary voltage $V_2(s)$ as the input variable instead of using the equivalent load resistance R_L. The dynamics of the T-type equivalent circuit in Fig. 1 can be expressed as follows:

$$\begin{bmatrix} I_1(s) \\ I_2(s) \end{bmatrix} = \begin{bmatrix} Y_{11}(s) & Y_{12}(s) \\ Y_{21}(s) & Y_{22}(s) \end{bmatrix} \begin{bmatrix} V_1(s) \\ V_2(s) \end{bmatrix} \tag{18}$$

where $Y_{11}(s)$, $Y_{12}(s)$, $Y_{21}(s)$, and $Y_{22}(s)$ are transfer functions from $V_1(s)$ and $V_2(s)$ to $I_1(s)$ and $I_2(s)$. The block diagram of the proposed model is shown in Fig. 8. Then, $I_2(s)$ is expressed as follows:

$$I_2(s) = Y_{21}(s)V_1(s) + Y_{22}(s)V_2(s). \tag{19}$$

From the circuit equations, $Y_{21}(s)$ and $Y_{22}(s)$ are described as follows:

$$Y_{21}(s) = \frac{I_2(s)}{V_1(s)} = \frac{b_3 s^3}{s^4 + a_3 s^3 + a_2 s^2 + a_1 s + a_0} \tag{20}$$

$$Y_{22}(s) = \frac{I_2(s)}{V_2(s)} = \frac{d_3 s^3 + d_2 s^2 + d_1 s}{s^4 + a_3 s^3 + a_2 s^2 + a_1 s + a_0} \tag{21}$$

where each coefficient is defined as follows:

$$a_3 = \frac{R_1 L_2 + R_2 L_1}{L_1 L_2 - {L_m}^2} \tag{22}$$

$$a_2 = \frac{R_1 R_2 + (L_1/C_2) + (L_2/C_1)}{L_1 L_2 - {L_m}^2} \tag{23}$$

$$a_1 = \frac{(R_1/C_2) + (R_2/C_1)}{L_1 L_2 - {L_m}^2} \tag{24}$$

$$a_0 = \frac{1}{C_1 C_2 (L_1 L_2 - {L_m}^2)} \tag{25}$$

$$b_3 = \frac{-L_m}{L_1 L_2 - {L_m}^2} \tag{26}$$

$$d_3 = \frac{L_1}{L_1 L_2 - {L_m}^2} \tag{27}$$

$$d_2 = \frac{R_1}{L_1 L_2 - {L_m}^2} \tag{28}$$

$$d_1 = \frac{1}{C_1 (L_1 L_2 - {L_m}^2)}. \tag{29}$$

The bode diagram of $Y_{21}(s)$ and $Y_{22}(s)$ is shown in Fig. 9. Since two out of three zeros of $Y_{22}(s)$ exist at the resonance frequency, the gain of $Y_{22}(s)$ is decreased at the resonance frequency. As a result, the harmonic components of $V_2(s)$ are not suppressed and have an effect on the harmonic distortion of $I_2(s)$.

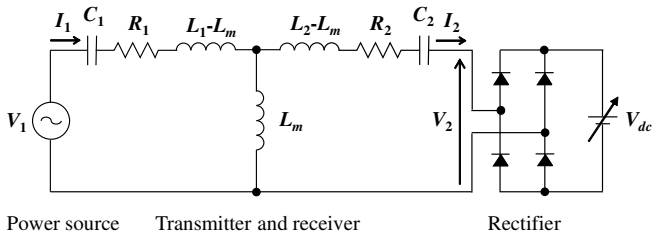

Fig. 10. Experimental circuit of the wireless power transfer system.

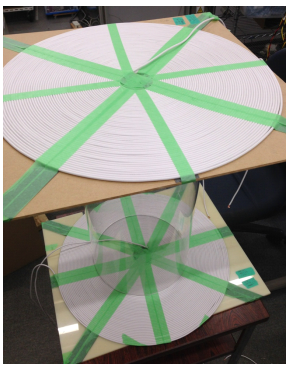

(a) Transmitter and receiver.

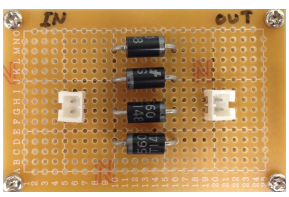

(b) Rectifier.

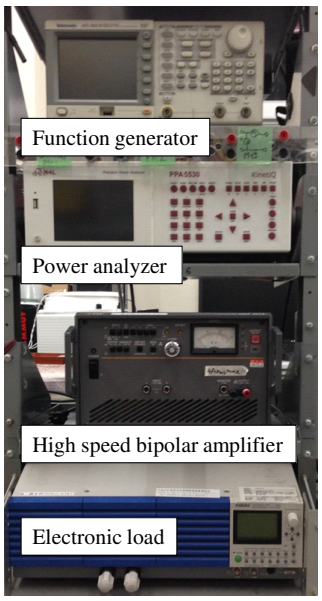

(c) Power source, load, and analyzer.

Fig. 11. Experimental equipment.

IV. Experiments

A. Experimental setup

The wireless power transfer system, which is indicated in Fig. 10, was built and tested. In order to eliminate the harmonic components caused by the primary voltage, a sine wave voltage source was used. Therefore, the harmonic current distortion is caused by only the diode rectifier, which generates the secondary voltage. In addition, the DC-DC converter was replaced by an electronic load, which simulated a constant voltage load.

The experimental equipment is shown in Fig. 11. The power source was composed of a function generator (AFG3021B, Tektronix) and a high speed bipolar amplifier (HSA4014, NF Corporation). The amplitude of the primary voltage V_1 was tuned to 10 V and the operating frequency was set to 99.6 kHz. The diode rectifier consisted of Schottky barrier diodes (SB560, Fairchild semiconductor). The amplitude of the DC link voltage V_{dc} was regulated by the electronic load (PLZ1004W, KIKUSUI). Waveforms of the secondary voltage and the secondary current were measured by a mixed signal oscilloscope (MSO3034, Tektronix) and their harmonics were analyzed by a power analyzer (PPA5530, Newtons4th Ltd.).

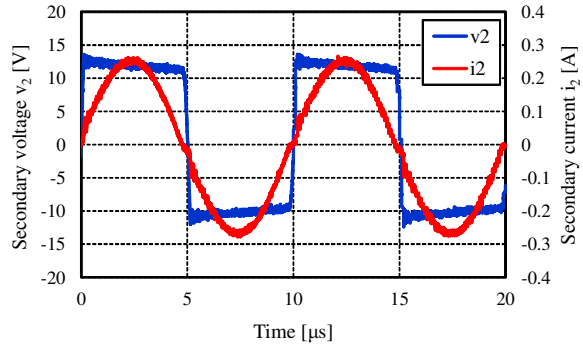

(a) V_{dc} = 10 V.

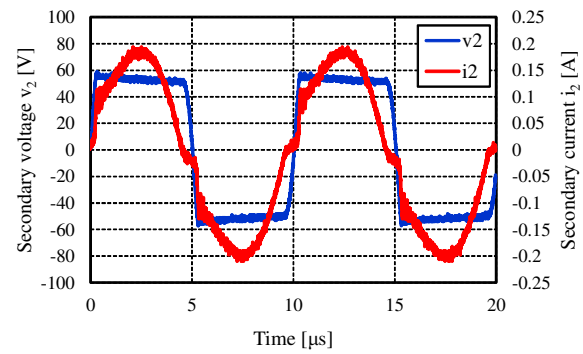

(b) V_{dc} = 50 V.

Fig. 12. Measured waveforms of the secondary voltage and the secondary current.

B. Experimental results

The measured waveforms are shown in Fig. 12. When the amplitude of V_{dc} is equal to 10 V, the waveform of the secondary current is close to a sine wave. On the other hand, when the amplitude of V_{dc} is set to 50 V, it is seen that the secondary current is distorted slightly at the zero-crossing because of the discontinuous state. Additionally, the secondary voltage and the secondary current are not in phase. This is caused by the harmonic components of the secondary voltage.

The total harmonic distortion (THD) of the secondary current is indicated in Fig. 13. As the amplitude of V_{dc} is increased, the secondary current has a higher proportion of the harmonic components. This result can be analyzed using the proposed model. When the amplitude of V_{dc} is larger than the amplitude of V_1, the secondary current is dominantly affected by $Y_{22}(s)$ due to eq. (19). Since $Y_{22}(s)$ cannot suppress the harmonic components of the secondary voltage, the harmonic components of the secondary current is increased.

Fig. 14 shows the harmonic component of the secondary current and indicates that the secondary current has odd-order harmonics. Therefore, it is verified that the secondary current is distorted by the harmonic components of the secondary voltage due to the diode rectifier.

In the case where the desired charging power is larger, the amplitude of V_{dc} has to be increased. Therefore, the charging power control should be designed considering the harmonic current distortion to achieve the desired charging power.

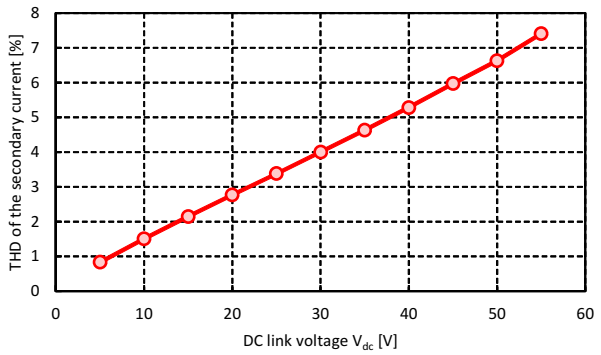

Fig. 13. Total harmonic distortion of the secondary current.

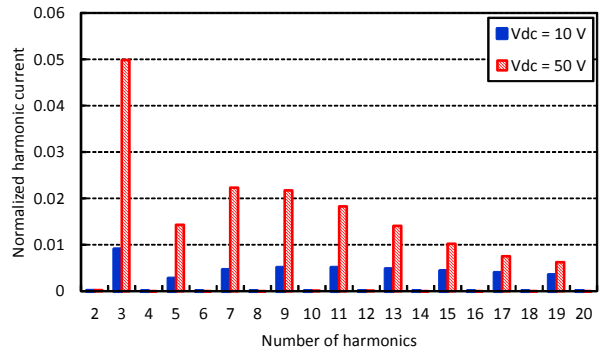

Fig. 14. Harmonic component of the secondary current.

V. Conclusion

This paper proposed a novel WPT circuit model using the secondary voltage as the input variable of transfer functions and analyzed the harmonic current distortion caused by the diode rectifier on the secondary side. Experiments demonstrated that the harmonic current distortion is increased with the increase in the ratio of the secondary voltage divided by the primary voltage. These results indicate that the charging power control should be designed with consideration for the harmonic current distortion.

In future works, the charging power control considering the harmonic current distortion will be proposed. In addition, the behavior of transfer functions, which are determined by the parameters of the transmitter and the receiver, will be analyzed.

References

[1] Y. Hori, "Future vehicle driven by electricity and control-research on four-wheel-motored "UOT electric march II"," *IEEE Transactions on Industrial Electronics*, vol. 51, no. 5, pp. 954–962, Oct. 2004.

[2] M. L. G. Kissin, J. T. Boys, and G. A. Covic, "Interphase mutual inductance in polyphase inductive power transfer systems," *IEEE Transactions on Industrial Electronics*, vol. 56, no. 7, pp. 2393–2400, Jul. 2009.

[3] J. Shin, S. Shin, Y. Kim, S. Ahn, S. Lee, G. Jung, S. Jeon, and D. Cho, "Design and implementation of shaped magnetic-resonance-based wireless power transfer system for roadway-powered moving electric vehicles," *IEEE Transactions on Industrial Electronics*, vol. 61, no. 3, pp. 1179–1192, Mar. 2014.

[4] A. Kurs, A. Karalis, R. Moffatt, J. D. Joannopoulos, P. Fisher, and M. Soljacic, "Wireless power transfer via strongly coupled magnetic resonance," *Science Express on 7 June 2007*, vol. 317, no. 5834, pp. 83–86, Jun. 2007.

[5] T. Imura, T. Uchida, and Y. Hori, "Flexibility of contactless power transfer using magnetic resonance coupling to air gap and misalignment for EV," *World Electric Vehicle Association Journal*, vol. 3, pp. 1–10, 2010.

[6] M. Kato, T. Imura, and Y. Hori, "New characteristics analysis considering transmission distance and load variation in wireless power transfer via magnetic resonant coupling," in *Proc. IEEE 34th International Telecommunications Energy Conference*, 2012, pp. 1–5.

[7] Y. Moriwaki, T. Imura, and Y. Hori, "Basic study on reduction of reflected power using DC/DC converters in wireless power transfer system via magnetic resonant coupling," in *Proc. IEEE 33rd International Telecommunications Energy Conference*, 2011, pp. 1–5.

[8] K. Iimura, N. Hoshi, and J. Haruna, "Experimental discussion on inductive type contactless power transfer system with boost or buck converter connected to rectifier," in *Proc. IEEE 7th International Power Electronics and Motion Control Conference*, 2012, pp. 2652–2657.

[9] M. Kato, T. Imura, and Y. Hori, "Study on maximize efficiency by secondary side control using DC–DC converter in wireless power transfer via magnetic resonant coupling," in *Proc. 27th International Electric Vehicle Symposium and Exhibition*, 2013, pp. 1–5.

[10] K. Hata, T. Imura, and Y. Hori, "Maximum efficiency control of wireless power transfer considering dynamics of DC–DC converter for moving electric vehicles," in *Proc. 30th Annual IEEE Applied Power Electronics Conference and Exposition*, 2015, pp. 3301–3306.

[11] S. Li and C. C. Mi, "Wireless power transfer for electric vehicle applications," *IEEE Journal of Emerging and Selected Topics in Power Electronics*, vol. 3, no. 1, pp. 4–17, Mar. 2015.

[12] T. Hiramatsu, X. Huang, M. Kato, T. Imura, and Y. Hori, "Wireless charging power control for HESS through receiver side voltage control," in *Proc. 30th annual IEEE Applied Power Electronics Conference and Exposition*, 2015, pp. 1614–1619.

[13] K. Hata, T. Imura, and Y. Hori, "Dynamic wireless power transfer system for electric vehicle to simplify ground facilities – power control based on vehicle-side information –," in *Proc. 28th International Electric Vehicle Symposium and Exhibition*, 2015, pp. 1–12.

[14] W. Zhang, S. C. Wong, C. K. Tse, and Q. Chen, "A study of sectional tracks in roadway inductive power transfer system," in *Proc. 2011 IEEE Energy Conversion Congress and Exposition*, 2011, pp. 822–826.

[15] H. H. Wu, A. Gilchrist, K. Sealy, and D. Bronson, "A 90 percent efficient 5kW inductive charger for EVs," in *Proc. 2012 IEEE Energy Conversion Congress and Exposition*, 2012, pp. 275–282.

[16] D. Gunji, T. Imura, and H. Fujimoto, "Fundamental research of power conversion circuit control for wireless in-wheel motor using magnetic resonance coupling," in *Proc. 40th Annual Conference of the IEEE Industrial Electronics Society*, 2014, pp. 3004–3009.

[17] J. G. Hayes, M. G. Egan, J. M. D. Murphy, S. E. Schulz, and J. T. Hall, "Wide-load-range resonant converter supplying the SAE J-1773 electric vehicle inductive charging interface," *IEEE Transactions on Industry Applications*, vol. 35, no. 4, pp. 884–895, Jul./Aug. 1999.

[18] H. H. Wu, G. A. Covic, J. T. Boys, and D. J. Robertson, "A series-tuned inductive-power-transfer pickup with a controllable AC-voltage output," *IEEE Transactions on Industrial Electronics*, vol. 26, no. 1, pp. 98–109, Jan. 2011.

[19] M. S. Chinthavali, O. C. Onar, J. M. Miller, and L. Tang, "Single-phase active boost rectifier with power factor correction for wireless power transfer applications," in *Proc. 2013 IEEE Energy Conversion Congress and Exposition*, 2013, pp. 3258–3265.

[20] T. Imura and Y. Hori, "Maximizing air gap and efficiency of magnetic resonant coupling for wireless power transfer using equivalent circuit and Neumann formula," *IEEE Transactions on Industrial Electronics*, vol. 58, no. 10, pp. 4746–4752, Oct. 2011.